fire

MDPI

Article

Comparative Analysis between Remote Sensing Burned Area Products in Brazil: A Case Study in an Environmentally Unstable Watershed

Juarez Antonio da Silva Junior [1], Admilson da Penha Pacheco [1], Antonio Miguel Ruiz-Armenteros [2,3,4,*] and Renato Filipe Faria Henriques [5]

1 Center for Technology and Geosciences, Department of Cartographic and Surveying Engineering, Federal University of Pernambuco, Av. Prof. Moraes Rego, 1235, Cidade Universitária, Recife 50670-901, PE, Brazil; juarez.silvajunior@ufpe.br (J.A.d.S.J.); admilson.pacheco@ufpe.br (A.d.P.P.)
2 Department of Cartographic, Geodetic and Photogrammetry Engineering, University of Jaén, Campus Las Lagunillas s/n, 23071 Jaén, Spain
3 Microgeodesia Jaén Research Group (PAIDI RNM-282), University of Jaén, Campus Las Lagunillas s/n, 23071 Jaén, Spain
4 Center for Advanced Studies on Earth Sciences, Energy and Environment CEACTEMA, University of Jaén, Campus Las Lagunillas, s/n, 23071 Jaén, Spain
5 Department of Earth Sciences, Institute of Earth Sciences (ICT), University of Minho (UMinho), Campus de Gualtar, 4710-057 Braga, Portugal; rhenriques@dct.uminho.pt
* Correspondence: amruiz@ujaen.es

Abstract: Forest fires can profoundly impact the hydrological response of river basins, modifying vegetation characteristics and soil infiltration. This results in a significant increase in surface flow and channel runoff. In response to these effects, many researchers from different areas of earth sciences are committed to determining emergency measures to rehabilitate river basins, intending to restore their functions and minimize damage to soil resources. This study aims to analyze the mapping detection capacity of burned areas in a river basin in Brazil based on images acquired by AMAZÔNIA-1/WFI and the AQ1KM product. The effectiveness of the AMAZÔNIA-1 satellite in this regard is evaluated, given the importance of the subject and the relatively recent introduction of the satellite. The AQ1KM data were used to analyze statistical trends and spatial patterns in the area burned from 2003 to 2023. The U-Net architecture was used for training and classification of the burned area in AMAZÔNIA-1 images. An increasing trend in burned area was observed through the Mann–Kendall test map and Sen's slope, with the months of the second semester showing a greater occurrence of burned areas. The NIR band was found to be the most sensitive spectral resource for detecting burned areas. The AMAZÔNIA-1 satellite demonstrated superior performance in estimating thematic accuracy, with a correlation of above 0.7 achieved in regression analyses using a 10 km grid cell resolution. The findings of this study have significant implications for the application of Brazilian remote sensing products in ecology, water resources, and river basin management and monitoring applications.

Keywords: remote sensing; forest fires; burned area; AMAZÔNIA1; AQ1KM

Citation: da Silva Junior, J.A.; Pacheco, A.d.P.; Ruiz-Armenteros, A.M.; Henriques, R.F.F. Comparative Analysis between Remote Sensing Burned Area Products in Brazil: A Case Study in an Environmentally Unstable Watershed. *Fire* **2024**, *7*, 238. https://doi.org/10.3390/fire7070238

Academic Editors: Giovanni Laneve and Darko Stipanicev

Received: 12 April 2024
Revised: 26 June 2024
Accepted: 5 July 2024
Published: 9 July 2024

1. Introduction

Brazil's natural vegetation comprises three distinct biomes: Tropical Forests, Cerrado, and Caatinga. These biomes collectively cover more than half of the country's territory. However, both the Cerrado and Caatinga are experiencing significant degradation due to human and natural activities, particularly fires. The majority of these fires are caused by human actions [1].

Research on global burned area remote sensing products commenced in the late 1980s to provide comprehensive global representations of fire occurrences and burned area extents. Chuvieco et al. [2] reviewed the physical principles underlying burned area

detection from satellite observations. They traced historical trends in the utilization of satellite sensors for burned area monitoring, summarized recent approaches to burned area mapping, and evaluated existing burned area products at both global and regional scales.

The FIRE_CCI project was initiated in 2012 to improve burned area mapping and utilize this information in global vegetation and atmospheric models [3]. Regional analyses have demonstrated that medium-resolution sensors have the potential to distinguish fire-affected areas [4,5]. Several studies have highlighted the impact of sensor spatial and temporal resolutions on the ability of satellites to detect burned areas [6–8]. Automatic mapping is hindered by challenges associated with coarse spatial resolution images, which are subject to variability in spectral characteristics in burned areas [8]. Although sensors with medium spatial resolution provide higher accuracy, their temporal resolutions may not be suitable for mapping tropical regions that are prone to cloud cover, as they may not be able to capture the necessary data on time [7–9].

The FIRE_CCI project is developing methods to generate global, long-term products that meet the needs of climate modelers, land managers, and local users in areas where local fire statistics are unavailable. The project has delineated the burned area information requirements for each user group in terms of coverage, accuracy, resolution, and delivery time. This research was supported by a comprehensive literature review. The review examined previous uses of datasets across a broad spectrum of topics, with a focus on those most pertinent to climate, carbon, and atmospheric models. Humber et al. [10] serve as a crucial reference in this field. Their study provides a synopsis of current global data products, outlining their uncertainties, limitations, and applications. It presents a summary of the user needs analysis based on a survey of over 47 questionnaires and concludes with a gap analysis that outlines future needs and requirements. This information will inform the development of global products in the coming decades [11].

The validation of satellite active fire products presents significant challenges due to the difficulty in collecting independent reference data capable of characterizing active fire locations and properties. It is of paramount importance to comprehend the sources of error that currently affect coarse burned area products to identify any algorithmic weaknesses [12].

Previous methodologies have relied on independent reference data collected from aircraft observations of prescribed fires and wildfires [4]. Conducting aerial campaigns in a regionally or globally representative manner can be expensive and challenging, particularly when coordinating with cloud-free conditions during satellite passages. Similarly, while ground-based fire measurements offer valuable insights, coordinating such efforts across vast areas presents logistical difficulties [13]. Although burned areas identified through high-spatial-resolution satellite data can validate active fire products, they may not reliably confirm the detection of such data during periods of inactivity or cloud cover, potentially omitting crucial information on active fire product errors. High-spatial-resolution ASTER data have been used to validate the MODIS Terra active fire product through the strategic integration of data collection from the same satellite, effectively addressing issues of timing and synoptic coverage.

This study presents a rigorous framework for comparing global fire products in terms of their spatial and temporal characteristics. The study focuses on four operational products: Copernicus Burned Area, Fire CCI, MODIS MCD45A1, and MODIS MCD64A1. The intercomparison carefully considers the temporal and spatial dimensions of these products, using a spatial and temporal analysis grid [14]. A non-overlapping grid of Thiessen scene areas (TSAs), which are generated from Landsat World Reference System (WRS-2) scene centroids, is employed to partition the data into monthly time intervals. This allows for the creation of three-dimensional analysis elements called voxels. The evaluation of burning within each voxel serves as an indicator of the total area burned. Additionally, comparison with MODIS active fire observations provides an independent measure of the timing accuracy of burned patches. The evaluation extends from 2005 to 2011 and includes all available data for all products [15].

The objective of this investigation is to provide Brazilian data users with relevant insights into the comparative effectiveness of available products for detecting burned areas. It identifies regions where forest fire detection exhibits variations in timing and magnitude. Forest fires have significant impacts on river basin transition areas between the Cerrado and Caatinga biomes. Therefore, it is essential to map and document the extent of these events. The primary objective of this study is to delineate burned areas using images sourced from AMAZÔNIA-1/WFI and the AQ1KM product, coupled with an assessment of their performance. The methodology employed integrates the U-Net semantic segmentation network to classify images from the AMAZÔNIA-1, alongside the Burned Area Index (BAI) and the Normalized Difference Vegetation Index (NDVI). The statistical analysis and validation process aims to quantify the accuracy of the classification, including both commission errors (CEs) and omission errors (OEs), as well as the Dice coefficient (DC). This research utilizes MapBiomas data with a spatial resolution of 30 m as a reference product to identify discrepancies, which will then inform the stratification strategies employed in future validation endeavors. This innovative approach not only provides Brazilian data users with relevant insights into the effectiveness of available products but also identifies regional variations in forest fire detection, particularly in the transition areas between the Cerrado and Caatinga biomes. This is the first study to assess the potential of AMAZÔNIA-1 scenes for mapping burned areas, employing semantic segmentation based on the U-Net architecture. Furthermore, the study takes full advantage of the AQ1KM product dataset, thus enabling, in a pioneering way, the analysis of temporal trends, with the potential to cover the entire South American region. The goal is to guarantee that the application accurately captures the relevant surface phenomena.

2. Materials and Methods

2.1. Study Area

The study area comprises three contiguous river basins situated within the transitional zone between the Cerrado and Caatinga biomes (Figure 1). The basins in question are part of the Ottocoded Hydrographic Base (BHO), which adheres to the Brazilian Systematic Mapping standards. This mapping delineates the boundaries of Brazil's river basins at varying scale levels and is utilized by the National Water and Basic Sanitation Agency (ANA) in the management of water resources. The BHO is created from the digital cartography of the country's hydrography and is organized to generate hydrologically consistent information, which is attributed to Otto Pfafstetter's basin coding [16].

The Amazon Environmental Research Institute (IPAHN) has estimated the river basin's area to be 74,517.23 km^2, encompassing the majority of the biomes' native vegetation remnants. However, the basin is also recognized as one of the world's hotspots for deforestation and forest fires [17]. The basin contains the sources of important Brazilian rivers, such as the Araguaia River and the Tocantins River. Currently, the region is undergoing a significant process of urbanization and expansion of pasture areas, in addition to housing large expanses of soybean plantations, which require an increasing use of water for irrigation. The study region has three power generation plants, the largest of which is the Boa Esperança Hydroelectric Plant, the largest in the state of Piauí with a combined production estimated at 9.9 million kilowatts. However, this production is threatened by increasingly frequent droughts.

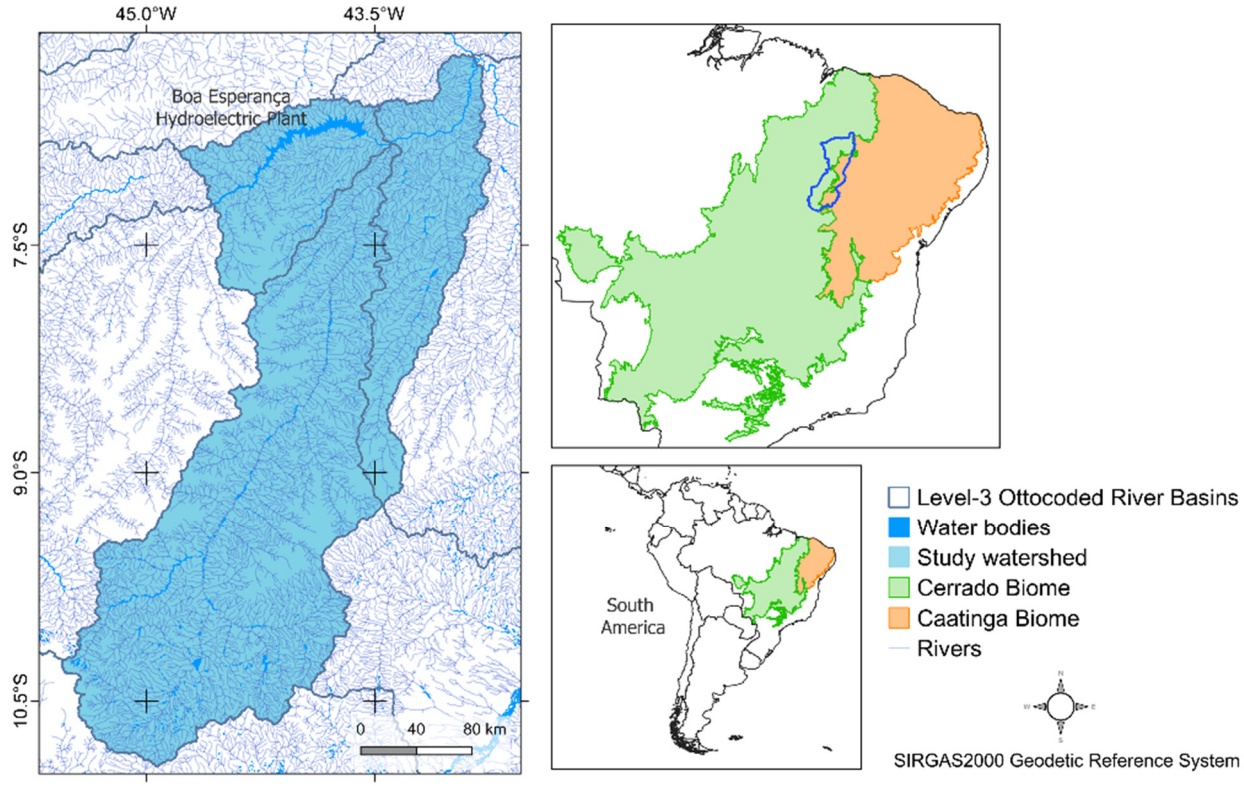

Figure 1. Study area. Delimitation of the Ottocoded Level-3 river basin located between the Caatinga and Cerrado biomes.

2.2. Satellite Data

2.2.1. AMAZÔNIA-1 Satellite Data

The study utilized orbital images captured by the Wide Field Imaging Camera (WFI) sensor, which is mounted on the AMAZÔNIA-1 satellite. The WFI is composed of four spectral bands: blue (0.45–0.52 µm), green (0.52–0.59 µm), red (0.63–0.69 µm), and near-infrared (NIR) (0.77–0.89 µm). The images have a ground sampling distance (GSD) of 64 m and were acquired at the preprocessing level (L4), which presents surface reflectance images, orthorectification, and georeferencing in the WGS84 geodetic reference system [18]. Image acquisition was facilitated by the United States Geological Survey (USGS) at http://earthexplorer.usgs.gov (accessed on 12 December 2023) [19]. Analyses were conducted using three cloud-free scenes dated 20 September 2021, 4 October 2022, and 13 October 2023, obtained from the study area. The AMAZÔNIA-1 images were used to compute the BAI and NDVI, which provided two additional parameters for detecting burned areas.

2.2.2. AQ1KM Satellite Data

The AQ1KM product is derived from data obtained from Collection 6 of MODIS, which was gathered simultaneously from the AQUA and TERRA satellites. The AQ1KM product is georeferenced and has a GSD of 1 km. The objective of this product is to provide a broad estimate and an overview of burned areas in Brazilian biomes [20]. The product was developed in collaboration with the Laboratory of Environmental Satellite Applications (LASA) at the Department of Meteorology of the Federal University of Rio de Janeiro (UFRJ). The product is based on a methodology that incorporates detailed spectral indices as described by Libonati et al. [21]. The data are made available monthly on the Terrabrasilis.dpi.inpe.br platform.

2.2.3. MapBiomas Fire

The MapBiomas project employed Landsat satellite image mosaics with a GSD of 30 m to map burned areas in Brazil. The mapping period spanned from 1985 to 2022, providing monthly and annual data on burn scars across Brazil. The MapBiomas institutions conducted a comprehensive process collaboratively, utilizing artificial intelligence. Machine learning algorithms were employed on the Google Earth Engine (GEE) and Google Cloud Storage platforms, which offer extensive cloud processing capacity. The methodology for data provision is organized within the GEE, categorized by biomes and other spatial units. Samples are collected in both burned and non-burned areas for algorithm training by regions, in addition to the use of auxiliary environmental maps and fire hotspot records from MapBiomas [22]. The data from the MapBiomas fire were obtained for the dates corresponding to the data from AMAZÔNIA-1 and AQ1KM, specifically in September and October for the years 2021 and 2022. For the year 2023, three scenes from the Landsat-9-OLI2 satellite (30 m resolution) were used on October 30, as a reference product. This was made possible by the method of photointerpretation of the burned areas.

2.3. Methodology

2.3.1. Trend Analysis

The non-parametric Mann–Kendall (MK) test was used to identify temporal trends in the time series of burned area, based on 0.3 degrees × 0.3 degrees sample plots [23,24]. This method facilitates the calculation of binary maps, ensures data homogeneity, and minimizes the effects of mixed pixels and incorrect records, thus allowing the analysis of regional spatial trends in the watershed. The direction of the trend is indicated by the Z sign. An increasing trend is considered significant if the positive Z value is greater than 1.96 (based on normal probability tables) at the 0.05 significance level. Conversely, if the negative Z value is less than −1.96, the trend is considered significantly decreasing [25]. Additionally, the mean and standard deviation were calculated for each grid pixel, as well as the maximum frequency of burned area. The maximum frequency was determined by the burned areas in grid pixels that exceeded the mean plus the standard deviation and were thus considered anomalies in the time series from 2003 to 2023. All analyses were based on monthly AQ1KM data, due to its extensive temporal distribution of burned area. The magnitude of the trend in the burned area time series was estimated using the Sen's slope methodology [26,27], as follows:

$$\beta = \text{median}\left(\frac{x_j - x_k}{j - k}\right) \quad (1)$$

where x_j and x_k denote the data values at times j and k, respectively, with $j > k$. A positive β value indicates an increasing trend magnitude in the time series data, while a negative value indicates a decreasing trend magnitude in the time series data.

2.3.2. Training Samples

A spectral data library was created by identifying burned areas through photointerpretation. The library consists of 1000 samples, each covering 3.6 ha, with an equal split of 500 samples for burned areas and 500 for non-burned areas. These samples were used as input during the classification stage of AMAZÔNIA-1 images. The selection of samples ensured full coverage of the polygon over the set of photointerpreted pixels for each class.

2.3.3. U-Net Model Classification

The U-Net neural network architecture, introduced by Ronneberger et al. [28], uses an encoder–decoder approach to semantically classify images. The encoder extracts feature maps from the input image, reducing spatial dimensions while increasing channels. Conversely, the decoder reverses this process, decreasing channels and increasing spatial dimensions. During the encoding process, the spatial resolution decreases at each step

due to down-sampling filters, while the spectral resolution increases [29]. Conversely, the decoding phase entails passing the image through additional hidden layers that reverse the encoding process. Consequently, with each step, the image undergoes a loss of spectral resolution while gaining spatial resolution, ultimately leading to the final classification [30].

The study utilized spectral bands blue, green, red, NIR, BAI, and NDVI as input layers, while the output layers classified images between 0 (non-burned area) and 1 (burned area). The proposed U-Net method employs an encoder with two dense layers, each with 64 units, and a final output layer with 4 units. The first dense layer uses the Rectified Linear Unit (ReLU) activation function, while the second layer utilizes the linear activation function. The model was trained using the Adam optimizer with a learning rate of 0.0001, and an analysis of 10 epochs was conducted using the Cross-Entropy Loss function. The training data were divided into two sets: 70% for training and 30% for testing. This division was employed to evaluate the U-Net algorithm's ability to map burned areas. The iteration that produced the best model weights was determined based on the validation loss. This loss function is a commonly used method to prevent overfitting the data [31]. The training and testing environment configuration for the model was implemented in Python 3.8, using the Jupyter Notebook 7.1.1 module.

2.3.4. Accuracy Analysis

The quality assessment of a thematic map derived from remote sensing typically involves a systematic comparison with other maps derived from the same method. One common approach to evaluating remote sensing data is through the use of error matrices, which result from spatially comparing the product in question with reference data. Following the training of the U-Net model, a comparison was conducted between the AMAZÔNIA-1 and AQ1KM maps and reference data, to establish a set of evaluation metrics to ensure the accurate handling of validation data by the burned area products. Error matrices, which depict areas of agreement and disagreement, were employed to provide widely used accuracy metrics for the evaluation of burned area products, including CE, OE, and DC [32].

The OE represents the proportion of burned pixels in the reference map that were not classified as burned in the burned area product. Similarly, the CE denotes the proportion of pixels classified as burned in the product that are not burned pixels in the reference map [26]. The DC provides an objective approach to integrating information from both the OE and CE into a single metric. It defines the probability of a classifier identifying a pixel as burned, either in the product or reference data. The DC represents the conditional probability that the other classifier will also identify the pixel in question as burned [33].

In addition, a comparison was conducted using simple regression between the proportion of grid cells with a coarse resolution of 10 km, as identified as burned by the AMAZÔNIA-1 and AQ1KM products, and the proportion of area detected by the reference data. The root mean square error (RMSE) and correlation coefficient were used as estimates for the analysis of spatial conformity between grid cells.

3. Results and Discussion

3.1. Analysis of the Distribution, Frequency, and Trends of Burned Area

Figure 2 depicts the monthly distribution of the burned area in the river basin under study during the period from 2003 to 2023 using AQ1KM data. A seasonal interannual pattern of the burned area can be observed in the graph, with the highest values predominantly concentrated in the second half of the year. From 2003 to 2006, the lowest values observed in the entire series were observed, below 1000 km^2, except for the peak recorded in October 2005, which reached approximately 1400 km^2.

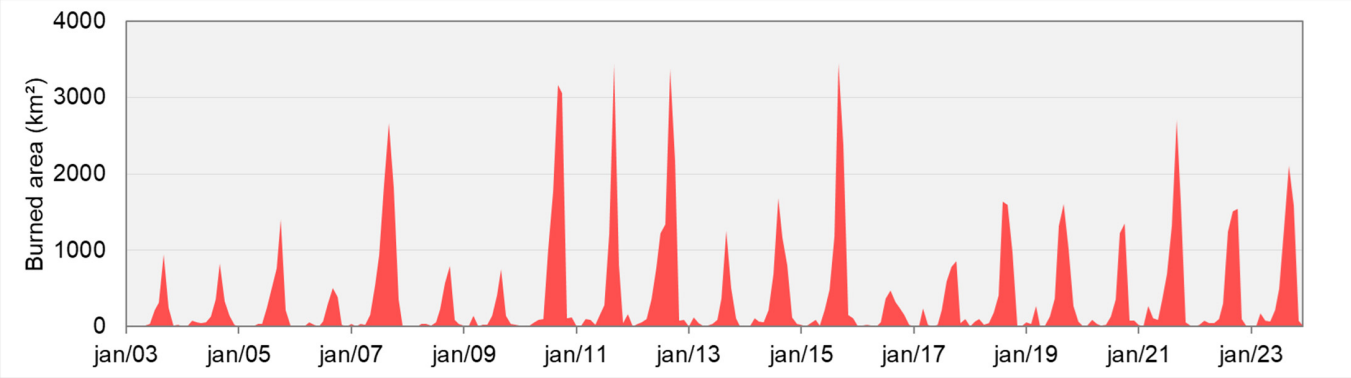

Figure 2. Area graph of the monthly burned area (km^2) in the river basin from 2003 to 2023.

This same pattern was observed in 2008 and 2009, following a historic peak in September 2007, with an area of approximately 2660 km^2, indicating that interannual variations in the burned area are abrupt, with significant peaks on a monthly scale. In other words, a single month can record a historic peak in the burned area. The second half of 2010, 2011, and 2012 was considered the most severe of the entire series, with significant peaks reaching 3000 km^2, especially in the months of September and October. In contrast, there was a significant decrease in estimates in the years 2013 and 2014, reaching approximately 35% and 37% compared to September 2012. In September 2015, the highest peak of the series was recorded, with approximately 3400 km^2, but with little variation compared to September 2011 and September 2012, which recorded 3300 km^2 and 3000 km^2, respectively. The years 2016 to 2023 exhibited a cyclical pattern, with fluctuations below 2300 km^2, devoid of pronounced peaks, except for September 2021, when the burned area reached 2704 km^2. Overall, the data indicate a statistically significant trend of increasing annual probability of wildfire occurrence in the watershed, with an angular coefficient of 0.032, a Z value of 2.805, and a Sen's slope of 0.2.

Despite the considerable variability observed in annual records of burned areas, the causes of these fires must be attributed to several factors, both natural and climatic. Once ignition sources have been established and active, climate variables become crucial for the occurrence of fires, directly influencing the functioning of the hydrological cycle of river basins [34]. It is noteworthy to highlight that the state of Piauí is included within the boundaries of the Drought Polygons, an area delineated by legislation in Decree-Law No. 63,778, dated 11 December 1968. This legislation identifies regions that are susceptible to recurring crises of prolonged drought, which requires special actions by part of the public sector [35]. One of the most severe crises recorded in the Brazilian Northeast occurred between mid-2007 and 2013, a period in which there was a significant increase in temperature anomalies and a reduction in precipitation, dam volume, river flow, and air and soil humidity. This situation was primarily attributable to the displacement of the Intertropical Convergence Zone (ITCZ) to a northern position than the historical average, due to the lack of sufficient warming of the waters of the South Atlantic, in addition to the formation of La Niña between 2009 and 2011 [36].

The same behavior was also observed by Moreira de Araújo et al. [37], who found that the frequent fire events observed in these years were characterized by strong La Niña events. These effects may be related to the main fire peaks in the region, as well as the native vegetation predominant in the transition region between the Cerrado and Caatinga biomes (Seasonal Forest). This vegetation is highly susceptible to the spread of fire in climates with high temperatures, as well as its spontaneous occurrence. Examples of this include Gorda Grass (*Melinis minutiflora*), a highly flammable invasive grass that grows quickly and accumulates large amounts of dry biomass during the dry season, and medium-sized trees such as Jurema-Preta (*Mimosa tenuiflora*) and Catingueira (*Poincianella piramidalis*), whose aerial parts are susceptible to fire [38]. According to the World Meteorological Organization

(WMO), the decade from 2001 to 2010 was the hottest globally since 1850, when temperature records began. The year 2010, with temperatures significantly above average in the northern region of South America, was the second hottest since 1998. Similarly, the effects of La Niña were more pronounced in 2007 and 2010 than those of El Niño, particularly in August [39]. CPTEC–INPE data indicate that the 2004–2005 and 2006–2007 periods were characterized by weaker El Niño events that did not significantly contribute to the occurrence of severe droughts, a primary factor in the fires. Nevertheless, in August 2007, the onset of a robust La Niña phenomenon commenced, persisting through the 2007–2008 period [37].

In combination with these phenomena, the impacts on the basin's hydrological cycle are further aggravated by human factors, such as the excessive use of fire to create pastures and plant crops. Silva et al. highlight that in the Brazilian Northeast, especially in the semi-arid region, 82.6% of the rural workforce is involved in family farming, despite several structural problems [40]. According to these authors, approximately half of the population does not utilize recommended agricultural practices and resorts to the controlled use of fire on vegetation as a method of clearing land for agricultural purposes. Some authors argue that burning vegetation in a controlled manner is a land management strategy, in addition to opening up space in the native forest, eliminating residues from deforestation and previous crops, and preparing the land for new plantations or livestock farming. Furthermore, they posit that this practice can confer benefits, including the elimination of pests and the provision of nutrients from ash, in addition to representing a rapid and cost-effective approach [40,41].

The peaks in burned areas observed in Figure 2, particularly between 2010 and 2014, may be associated with the reduction in the area of native forests through the use of methods that employ fire to expand agricultural areas [41]. According to data from MapBiomas, from 2000 to 2013, there was a 48% increase in agricultural areas in the river basin under study, predominantly in soil and pasture [22]. Moreover, there was a notable increase in the availability of agricultural financing during this period, with a 67% growth in credit lines for small and large producers between 2006 and 2017, and a total of BRL 404 billion allocated to the Safra Plan between 2010 and 2013. Despite the holding of the Rio+20 Conference in 2012 and the implementation of the New Forest Code (Law No. 12,651/12) in the same year, this period was also marked by the loosening of Brazilian environmental policy. This included the interruption of the creation and reduction processes of conservation units, in addition to the reduction of IBAMA's supervisory power against deforestation and forest fires [42–44].

Figure 3 presents the monthly frequency of burned areas per year in the river basin under study, from 2003 to 2023, based on AQ1KM data. The designation "low" is applied to locations with a low or no incidence of burned areas, while "high" is used to indicate locations with a frequency of four or more occurrences of burned areas throughout the time series.

It is observed that the monthly frequency of burned areas follows a well-defined pattern of periods of low and high incidence of forest fires. In the first months of the year, there are practically no fires. However, as the second half of the year approaches, we are beginning to see a significant increase in the number of fires. The initial records of burned areas in the series are concentrated in the northern sector of the basin, primarily along the deforestation arc, where human activity is intense due to agriculture around the Boa Esperança dam, the largest in the state of Piauí. This clearly demonstrates the anthropogenic ignition of fires in this region. Between the months of July and October, there is a significant occurrence of burned areas, which spreads from north to south. For example, in September, the same area can be burned up to 15 times, as indicated by the redder areas. Conversely, from November onwards, and particularly in December, the frequency of fires decreases significantly, with less than four occurrences being recorded (Figure 3).

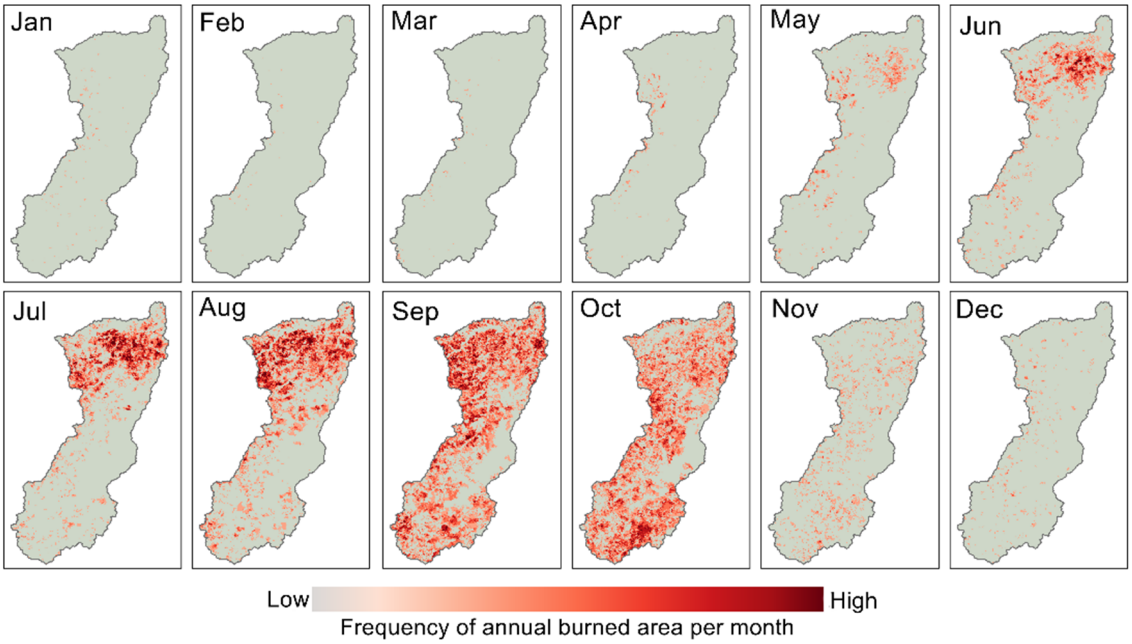

Figure 3. Spatial distribution of annual frequency of burned area per month.

In general, fires in Brazilian territory reach their peak intensity, especially in the Cerrado, during the months of July, August, and September. Between May and September, the Cerrado records the lowest levels of relative humidity, due to the drastic reduction in rainfall, the increase in air temperature, and the greater incidence of solar radiation throughout the day [45]. These favorable environmental conditions, in conjunction with the abundance of fine combustible materials (such as grasses, living or dead leaves, and thin twigs with a diameter of approximately 6 mm) present in the environment, both from the herbaceous layer and exotic species (e.g., *Brachiaria decumbens*), contribute to the occurrence of fires [37].

Despite the occurrence of burned areas in the first months of the year, it is not possible to observe an intensification in the frequency of these fires. This may be related to the rainfall regime, which is greater at this time of year, in addition to coinciding with the planting period of diverse cultures. In this context, the results observed are consistent with those presented in [40] and [46], which indicate that fires in the region are concentrated in seasons with low levels of rainfall and air humidity. Furthermore, the time series researched depicts the seasonality of fire occurrences in the vegetation of the studied region. Regardless of whether they are caused by humans or not, the occurrences are predominant in the months of June, July, August, September, October, and November. This is a consequence of a series of factors already mentioned, such as anthropogenic, meteorological, physical, and environmental factors [47]. In fact, fires in the Cerrado and Caatinga are highly seasonal. During the rainy season, from October to April, there is a significant increase in the amount of biomass. In the dry season, from May to September, the biomass becomes highly flammable and susceptible to the rapid spread of fire across vast areas of natural vegetation [48].

Figure 4 illustrates the spatial variation of the mean value, standard deviation, maximum frequency, Z value of the MK test, and Sen's slope of the annual trend of burned area during 2003–2023, using AQ1KM data. The grids are 0.3 degrees × 0.3 degrees in size, and the observed trends are statistically significant at the 95% confidence level.

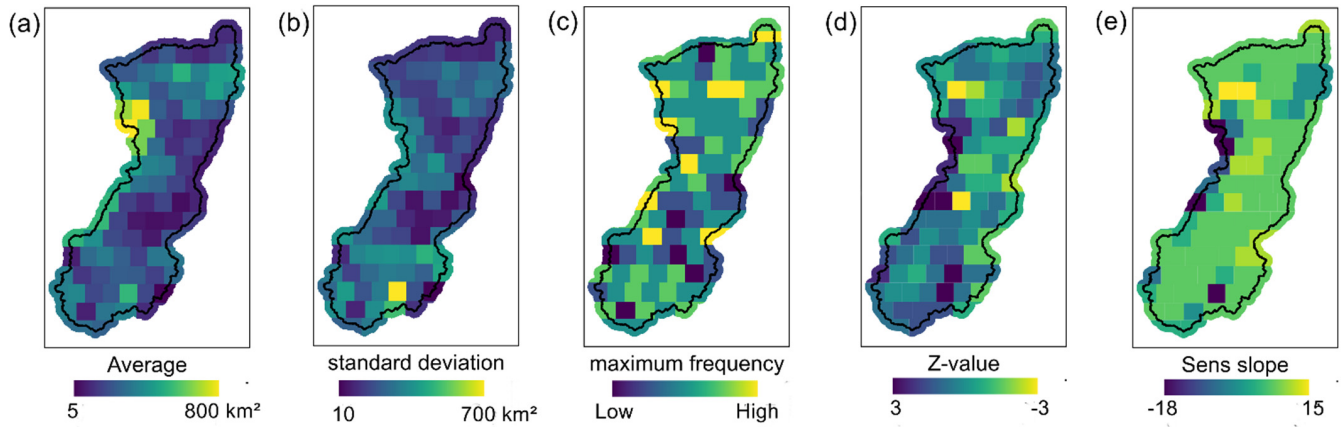

Figure 4. Map of mean (**a**), standard deviation (**b**), maximum frequency (**c**), trend by Z value (**d**), and Sen's slope (**e**) for the burned area grid based on the years 2003 to 2023.

The basin exhibited an overall annual average burned area of 257.8 km^2, with a minimum of 5 km^2 located in the central sector and on the eastern edges, and a maximum of 800 km^2, visually concentrated in the western sector. The annual standard deviation did not exhibit a discernible pattern, with 64% of grid pixels below 250 km^2 and a maximum point located in the lower sector of the basin, indicating high local variability and, consequently, an area that requires monitoring by environmental managers.

Figure 4 illustrates the spatial trend patterns of the gridded burned area through the Z value, which ranges from −3 to 3. Positive values indicate an "increasing trend", while negative values indicate a "decreasing trend". The results show that the majority of grids in the basin (65%) recorded an increasing trend, with maximum Z values scattered, except in some grids in the western sector of the basin. Furthermore, the basin exhibited a consistent distribution of burned area grids above the historical frequency, as evidenced by the yellowish pixels, which indicated points of attention for local burned area anomalies. During the period from 2003 to 2023, 10 points exhibited a burned area approximately 5 times above the historical standard deviation, and 24 grid pixels presented extreme burned areas at least 4 times above the historical standard deviation.

The Sen's slope map indicates a positive slope in the majority of the basin grids, with values predominantly above 10. However, it also presents strong negative slopes, indicating a low growth trend in the burned area. Figure 4a additionally depicts the highest averages, indicating that, although there is a tendency for the burned area to decrease, the burning estimates remain high. This indicates a necessity for further analysis to identify potential statistical stabilization.

3.2. Spectral Separability Analysis

Figure 5 presents boxplot graphs for the AMAZÔNIA-1, BAI, and NDVI bands for the pixel data samples from burned and unburned areas for the years 2021, 2022, and 2023.

It is observed that the visible bands did not present significant variations in the median between the burned and unburned classes in all years. Of particular interest is the blue band, which in the years 2021 and 2023 presented the same median value, approximately 0.15 and 0.28 for both classes, respectively. In contrast, the NIR band and the NDVI exhibited the most pronounced differences in the median, particularly in the year 2023, reaching a value of 0.24 for both. However, the NDVI presented a high standard deviation for the unburned class, with the minimum point situated close to the median of the burned NDVI. The BAI exhibited a comparable pattern to the NIR, though it exhibited instability in the median values in 2021, with values of 0.26 in 2021, 0.07 in 2022, and 0.08 in 2023.

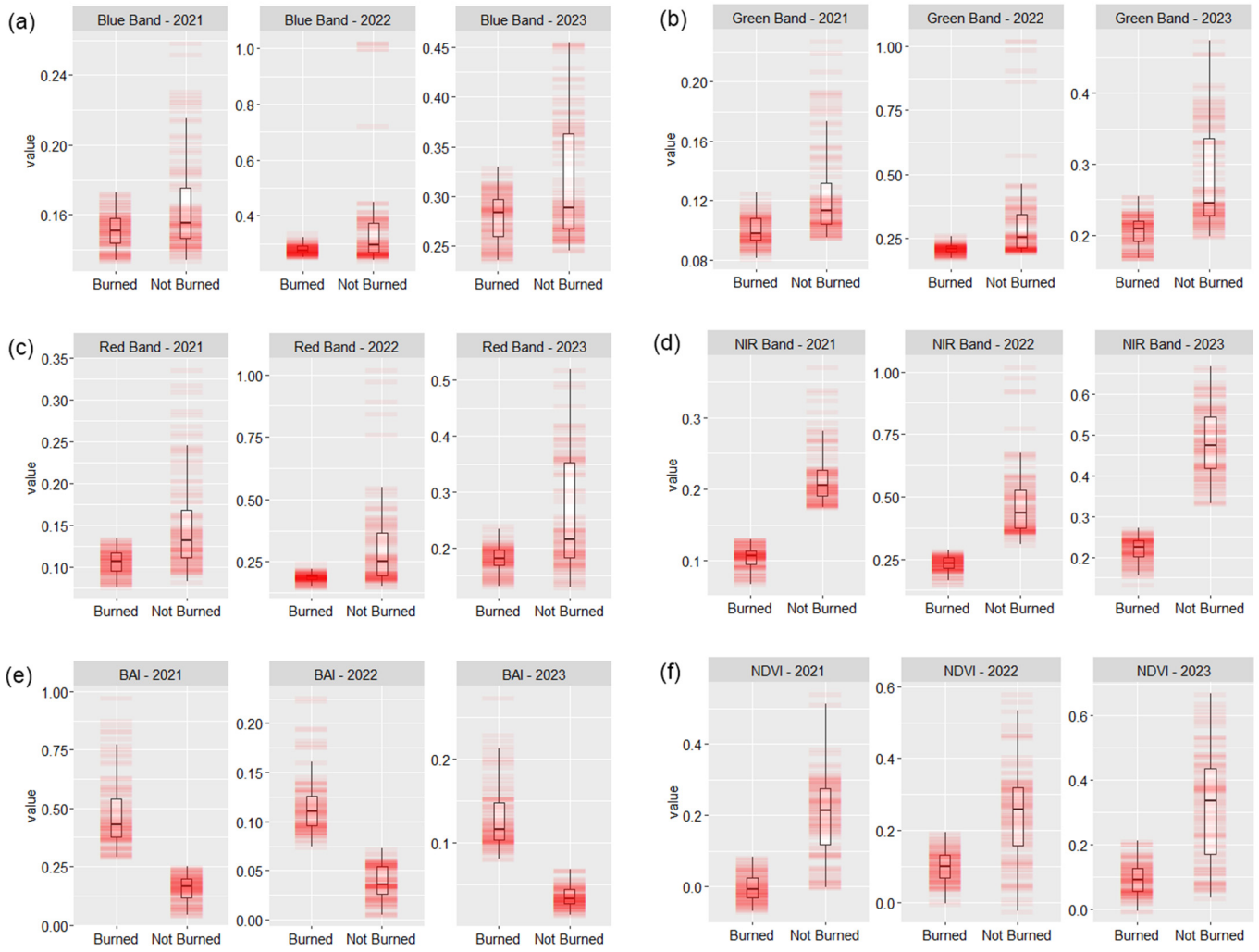

Figure 5. Boxplot of the sample pixel values of the burned and unburned areas of the AMAZÔNIA-1 blue (**a**), green (**b**), red (**c**), NIR (**d**), BAI (**e**), and NDVI (**f**) bands for the years 2021, 2022, and 2023.

In summary, the results demonstrate that AMAZONIA-1's unitary visible bands present certain limitations in detecting burned areas, which is a common occurrence in multispectral scenes. As previously stated in the literature, the visible bands have reduced sensitivity to heat, are susceptible to atmospheric interference, and encounter difficulties in distinguishing different types of land cover and fire scars [2,49,50]. Conversely, for image classification and photointerpretation, the composition of these bands provides a strong indicator for the identification of burned areas. The NIR band and the derived spectral indices (NDVI and BAI) have been demonstrated to be satisfactory in the detection of forest fires, given that this band is spectrally sensitive to variations in the state of the vegetation [51,52].

3.3. Burned Area by U-Net Classification

Figure 6 shows the U-Net training curves (epoch × loss) for AMAZÔNIA-1 spectral data samples for the years 2021, 2022, and 2023.

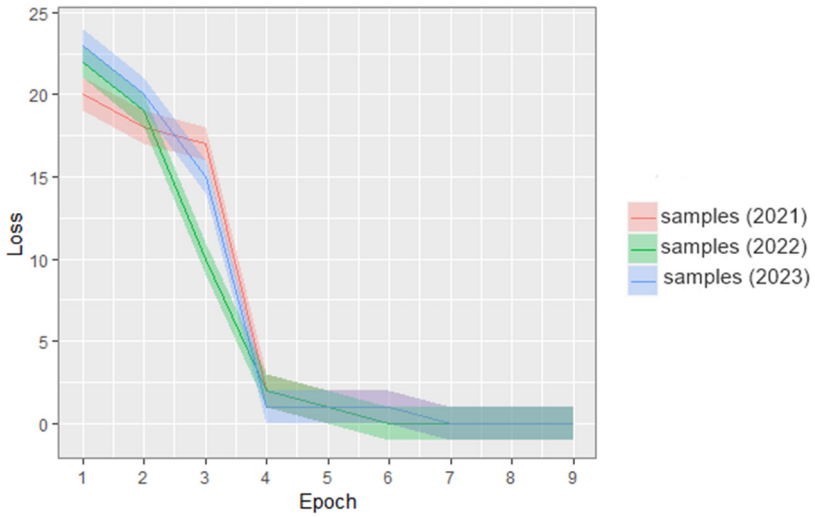

Figure 6. Training curves for U-Net classification.

The U-Net model was trained using spectral data from AMAZÔNIA-1, and a loss analysis was performed for the hydrographic basin under study to classify burned and unburned areas. The results demonstrated that the dataset underwent a significant adjustment in the fourth epoch and subsequently stabilized from the fifth epoch onwards. The loss value was found to be close to 0, thus demonstrating absolute stability for all tests conducted with five epochs. The lowest loss estimate was presented for each test. This analysis was of significant importance, as it enabled the identification of an optimal hyperparameter configuration for the dataset, while simultaneously avoiding overfitting, reducing computational cost, and minimizing processing time.

3.4. Accuracy Analysis

Figure 7 presents the spatial distribution of CE and OE in the classification of burned areas in the river basin for the years 2021, 2022, and 2023 for the sample examples of AMAZÔNIA-1 and AQ1KM.

The extent of the burned areas varied, influencing the degree of spatial conformity of the reference data. For instance, smaller burned areas (<10 km^2) led to an increase in CE and OE in both AQ1KM and AMAZÔNIA-1, while larger (>10 km^2) and more compact areas demonstrated satisfactory compliance (Figure 7). Overall, AMAZÔNIA-1 exhibited the lowest error estimates and a commendable performance in DC. Nevertheless, the two databases exhibited comparable error values, as evidenced by the CE for 2023, where AMAZÔNIA-1 was 38.5% and AQ1KM was 43.4%. Furthermore, a pattern was observed in CE and OE, with values that were relatively close to each other. This was similar to the pattern observed in 2022, where there was a variation of approximately 7.5% for AMAZÔNIA-1 and 4% for AQ1KM. DC also showed a pattern over the years, with the lowest values observed in 2021 and the highest values observed in 2023 for both datasets.

Overall, a deficiency is related to the acquisition time of the AMAZÔNIA-1 image. For 2021, there was an advance of 11 days, for 2022, an advance of 4 days, and for 2023, an advance of 13 days in relation to the acquisition time of the reference product which is a monthly compilation. This discrepancy may explain the CE and OE values observed. In environmentally unstable areas, such as when comparing maps of burned areas, even a difference of a few days can be crucial for a quality analysis [53]. Melchiorre and Boschetti [54] concurred with our analysis by calculating burned area persistence time to estimate the period during which burned areas are detectable using remote sensing change detection. The authors highlighted that the persistence time of the burned area varied considerably in time and space, differing between terrains. The authors observed that the variability in the persistence times of burned areas differed not only between land cover classes but also within and between the same class, depending on the biome and spectral domain. They

noted that the persistence times of burned areas in grasslands and savannas (similar to the Cerrado and Caatinga) were short and relatively uniform due to the fine fuels and fuel loads typical of fires in these areas. De Carvalho et al. [55] demonstrated in studies carried out in the Cerrado that the average dates reported for fire scars allow accurate detection within 1 day for large fires and typically within 2 days for small to medium-sized fires. This finding highlights the importance of using the most appropriate products for burned areas. However, the 1 km spatial resolution of AQ1KM increased detection errors in relation to AMAZONIA-1, showing better EO and EC values.

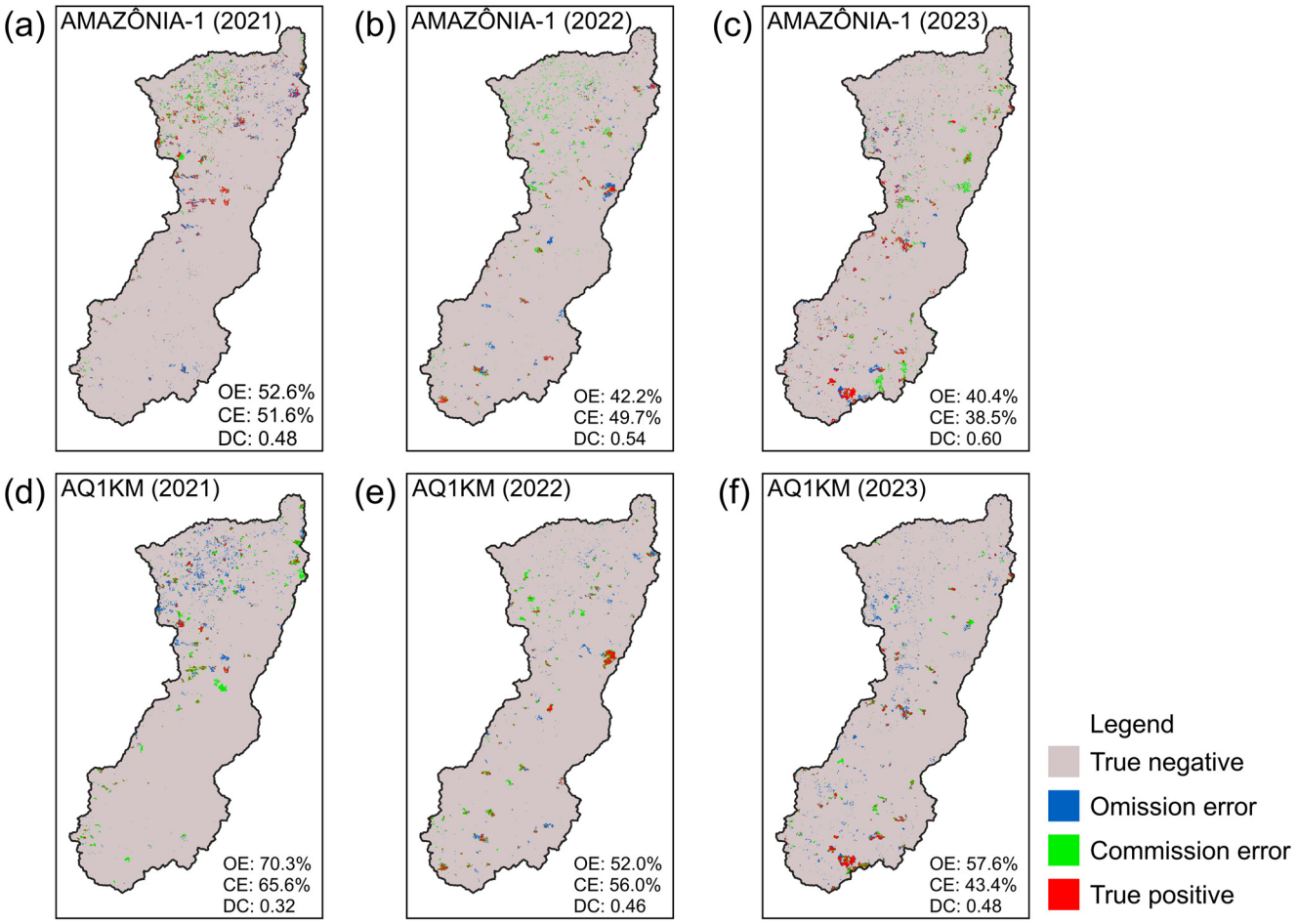

Figure 7. Spatial distribution of classification errors in the study area. (**a**–**c**) for AMAZÔNIA-1, and (**d**–**f**) for AQ1KM.

In contrast, another deficiency that can be observed in both datasets is related to low-severity fire events. For AMAZONIA-1, despite the spatial resolution (64 m), low-severity fires and vegetation in the post-burn regeneration phase can cause CE and OE, respectively, in their detection. This is because the affected vegetation has high sensitivity in the Short Wavelength InfraRed (SWIR) band, which is not included in AMAZÔNIA-1, and the visible bands, as previously mentioned. This limits the capacity of the system for detecting targets at this burn stage [56]. Although the NIR band is included and BAI and NDVI are employed as supporting resources, these three spectral resources may still be inadequate for detecting low-severity fires and vegetation in the regeneration phase. Campagnolo et al. [57] demonstrated that the Cerrado and Caatinga biomes can be used as a representative of other savanna-like biomes to improve operational mapping of burned areas. The study found that combining appropriate temporal, spatial, and spectral resolutions can lead to more accurate results. In particular, the study highlights the necessity for an Earth observation instrument with daily global coverage, a GSD exceeding 250 m,

and a bandwidth of 2.1–2.2 µm. The shortcomings identified in the AMAZONIA-1 dataset are also evident in the AQ1KM product, with the latter exhibiting a more pronounced deficiency due to its low spatial resolution. It is, however, important to note that the AQ1KM product is based on MODIS Level 1B 1 km V5 scenes, which include NIR and SWIR bands. These bands are sensitive to the spectral signal of areas that have been burned at different stages and are capable of detecting changes in vegetation health during periods of weekly aggregated scenes [21]. The linear regression for analyzing the spatial conformity between the AMAZÔNIA-1 and AQ1KM products and the reference data is shown in Figure 8, which depicts the results in a 10 km x 10 km pixel proportion grid.

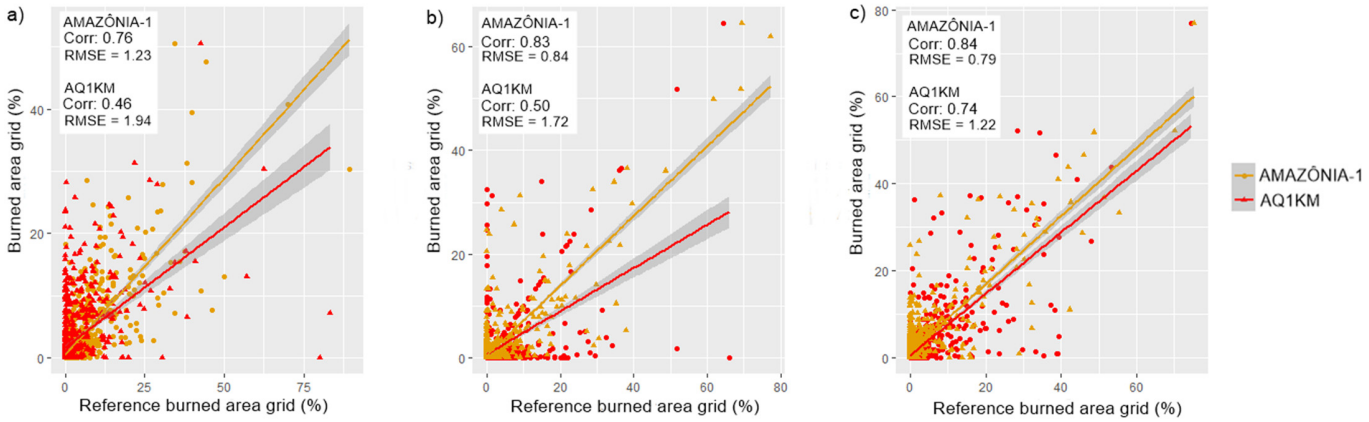

Figure 8. Linear regression by 10 km × 10 km grid proportion between the AQ1KM product and AMAZÔNIA-1, labeled as burned by independent reference data for the years (**a**) 2021, (**b**) 2022, and (**c**) 2023.

The correlation and RMSE values for the pixel grid regression exhibited a similar pattern of behavior for the CE and OE. The most favorable performance was slightly observed for AMAZÔNIA-1, with correlations above 0.7 for all years and RMSE values close to 1. In contrast, AQ1KM presented correlation values below expectations, particularly in 2019, with a correlation of <0.5 and RMSE > 1. However, there was an improvement in 2023. Conversely, the analysis of the results based on the 10 km × 10 km grid reduced the high dispersion of the smaller proportion areas. As illustrated in the graph, grid pixels with an aspect ratio below 30% exhibited a greater fit to the straight line, as in 2019 and 2023, approximately below 40%.

To achieve higher accuracy in the classification of satellite images, we employed the U-Net network. The network structure proposed in this study is based on a fully convolutional architecture, which preserves semantic information integrity to produce clearer and more accurate results. The U-Net classification algorithm proved instrumental in detecting data from the AMAZÔNIA-1 satellite, which is of particular importance for Brazil due to its vast territory, which is often obscured by clouds for a significant portion of the year. As demonstrated by Piao and Liu [58], the high-performance algorithm notably enhanced fire detection even in challenging conditions and in the absence of supplementary spectral resources. This is of particular significance in our study area, which is characterized by a multitude of spectral complexities, including cloud shadows, topography-induced shadows, and bodies of water, that can be mistaken for burned areas.

The MapBiomas data proved to be an invaluable reference product for research and development. They were particularly useful in analyzing different patterns and mutually validating them through spatial analysis. The potential of the MapBiomas product for mapping and validating burned areas was also recognized. However, the developers noted that future adjustments are necessary for tropical regions [59]. Therefore, global products remain a reliable source for operationalizing and analyzing socio-environmental losses

associated with tropical forest fires, in the absence of a national product that does not require algorithm adjustments [9,60,61].

It is pertinent to note that the frequency and statistical trend analysis conducted in this article has enabled the identification of recurring patterns of fires over time, particularly in the northern sector of the river basin. Furthermore, it has provided insight into the factors that influence these events and the precise observation of the months with the highest occurrence of fires, especially in the second half of the year. This information can guide managers on where to act more intensively and how to allocate resources to combat and prevent fires.

4. Conclusions

This study compares two national burned area mapping products, AMAZÔNIA-1 and AQ1KM, concerning their agreement and disagreement on spatial and temporal scales. The focus is on river basins located in a transition area between the Cerrado and Caatinga biomes, which frequently change land use and coverage. These changes affect the functioning of the region's water resources. The analysis is limited to temporal coverage of area burned products and reveals significant variations in estimates of total area burned, location, frequency, and timing of burning. The results of this research can guide future stratification strategies for validation efforts, ensuring the accurate capture of environmental impact phenomena through national remote sensing datasets and products.

It is of the utmost importance to have accurate information regarding the extent and distribution of burned areas, as this is crucial for regional and global environmental studies, as well as firefighting efforts. The increasing availability of medium-spatial-resolution satellite data presents new opportunities for regional burned area monitoring, both independently and in support of low-resolution monitoring.

Despite certain limitations, the data obtained from AMAZÔNIA-1 and AQ1KM proved to be highly effective in identifying fire-affected areas, providing significant spatial and temporal analysis capabilities. The AMAZÔNIA-1 satellite is capable of identifying burned areas exhibiting different patterns, as it has specific bands to obtain spectral indices of burns and vegetation. Furthermore, its spatial resolution and extensive coverage permit the detection of burned areas of smaller extents. The area covered by the satellite is approximately 850 km. Conversely, AQ1KM, with its extensive historical database on burned areas, enables the conduct of time series statistics and the identification of patterns, not only for Brazil but also for the entirety of South America. It is noteworthy that the Program team Queimadas from INPE has indicated that the AQ1KM product is currently undergoing validation, at a provisional maturity level. Furthermore, product quality control is underway. Finally, the methodology employed in this study demonstrates its utility in the creation of maps and the acquisition of information that identifies areas of native vegetation and springs affected by fire. This has enhanced our understanding of the effects of fire in river basins with a high anthropogenic impact and has improved our ability to monitor water resources in the Cerrado and Caatinga biomes, with potential applicability to other biomes as well.

Author Contributions: Conceptualization, J.A.d.S.J. and A.d.P.P.; methodology, J.A.d.S.J. and A.d.P.P.; software, J.A.d.S.J. and A.d.P.P.; validation, J.A.d.S.J., A.d.P.P., A.M.R.-A. and R.F.F.H.; formal analysis, J.A.d.S.J., A.d.P.P., A.M.R.-A. and R.F.F.H.; investigation, J.A.d.S.J., A.d.P.P., A.M.R.-A. and R.F.F.H.; resources, J.A.d.S.J. and A.d.P.P.; data curation, J.A.d.S.J.; writing—original draft preparation, J.A.d.S.J.; writing—review and editing, J.A.d.S.J., A.d.P.P., A.M.R.-A. and R.F.F.H.; visualization, J.A.d.S.J., A.d.P.P., A.M.R.-A. and R.F.F.H.; supervision, J.A.d.S.J., A.d.P.P., A.M.R.-A. and R.F.F.H.; project administration, J.A.d.S.J., A.d.P.P., A.M.R.-A. and R.F.F.H.; funding acquisition, J.A.d.S.J., A.d.P.P., A.M.R.-A. and R.F.F.H. All authors have read and agreed to the published version of the manuscript.

Funding: This research was supported by "Sensoriamento Remoto Aplicado no Estudos de Focos de Calor em Florestas do Brasil e Península ibérica" project (Pró-Reitoria de Pesquisa e Inovação (PROPESQi)—Universidade Federal de Pernambuco, Brazil (DECART/UFEPE), Ref.: SIPAC 23076.026035/2023-72), as well as by Portuguese national funding awarded by FCT—Foundation

for Science and Technology, I.P., projects UIDB/04683/2020 and UIDP/04683/2020. In addition, this research was also supported by POAIUJA 2023-24 and CEACTEMA from the University of Jaén (Spain), and RNM-282 research group from the Junta de Andalucía (Spain).

Institutional Review Board Statement: Not applicable.

Informed Consent Statement: Not applicable.

Data Availability Statement: All data and codes used in the current study are available upon request from the corresponding author.

Acknowledgments: We thank the authors and institutions involved for supporting this research.

Conflicts of Interest: The authors declare no conflicts of interest.

Abbreviations

This section provides a list of acronyms and abbreviations used in the text.

Acronyms	Meaning
ANA	National Water and Basic Sanitation Agency
BAI	Burned Area Index
BHO	Ottocoded Hydrographic Base
Corr	Correlation
CE	Commission Error
DC	Dice Coefficient
GEE	Google Earth Engine
GSD	Ground Sampling Distance
IPAHN	Amazon Environmental Research Institute
ITCZ	Intertropical Convergence Zone
LASA	Laboratory of Environmental Satellite Applications
MK	Mann–Kendall
MODIS	Moderate-Resolution Imaging Spectroradiometer
NIR	Near-Infrared
NDVI	Normalized Difference Vegetation Index
OE	Omission Error
OLI-2	Operational Land Instrument 2
ReLU	Rectified Linear Unit
RMSE	Root Mean Square Error
SWIR	Short-Wave Infrared
UFRJ	Federal University of Rio de Janeiro
TSA	Thiessen Scene Area
WFI	Wide Field Imaging Camera
WMO	World Meteorological Organization

References

1. INPE. Usos e Aplicações—INPE/Missão Amazonia. 2021. Available online: http://www.inpe.br/amazonia1/usos_aplicacoes.php (accessed on 19 March 2024).
2. Chuvieco, E.; Mouillot, F.; van der Werf, G.R.; San Miguel, J.; Tanase, M.; Koutsias, N.; García, M.; Yebra, M.; Padilla, M.; Gitas, I.; et al. Historical background and current developments for mapping burned area from satellite Earth observation. *Remote Sens. Environ.* **2019**, *225*, 45–64. [CrossRef]
3. Chuvieco, E.; Sandow, C.; Guenther, K.P.; González-Alonso, F.; Pereira, J.M.; Pérez, O.; Bradley, A.V.; Schultz, M.; Mouillot, F.; Ciais, P. Global Burned Area Mapping from European Satellites: The Esa Fire_Cci Project. *Int. Arch. Photogramm. Remote Sens. Spatial Inf. Sci.* **2012**, *XXXIX-B8*, 13–16. [CrossRef]
4. Ramo, R.; Roteta, E.; Bistinas, I.; van Wees, D.; Bastarrika, A.; Chuvieco, E.; van der Werf, G.R. African burned area and fire carbon emissions are strongly impacted by small fires undetected by coarse resolution satellite data. *Proc. Natl. Acad. Sci. USA* **2021**, *118*, e2011160118. [CrossRef] [PubMed]
5. Roteta, E.; Bastarrika, A.; Padilla, M.; Storm, T.; Chuvieco, E. Development of a Sentinel-2 burned area algorithm: Generation of a small fire database for sub-Saharan Africa. *Remote Sens. Environ.* **2019**, *222*, 1–17. [CrossRef]
6. Franquesa, M.; Vanderhoof, M.K.; Stavrakoudis, D.; Gitas, I.Z.; Roteta, E.; Padilla, M.; Chuvieco, E. Development of a standard database of reference sites for validating global burned area products. *Earth Syst. Sci. Data* **2020**, *12*, 3229–3246. [CrossRef]

7. Long, T.; Zhang, Z.; He, G.; Jiao, W.; Tang, C.; Wu, B.; Zhang, X.; Wang, G.; Yin, R. 30 m Resolution Global Annual Burned Area Mapping Based on Landsat Images and Google Earth Engine. *Remote Sens.* **2019**, *11*, 489. [CrossRef]
8. Pessôa, A.C.M.; Anderson, L.O.; Carvalho, N.S.; Campanharo, W.A.; Junior, C.H.L.S.; Rosan, T.M.; Reis, J.B.C.; Pereira, F.R.S.; Assis, M.; Jacon, A.D.; et al. Intercomparison of Burned Area Products and Its Implication for Carbon Emission Estimations in the Amazon. *Remote Sens.* **2020**, *12*, 3864. [CrossRef]
9. Shimabukuro, Y.E.; Dutra, A.C.; Arai, E.; Duarte, V.; Cassol, H.L.G.; Pereira, G.; Cardozo, F.d.S. Mapping Burned Areas of Mato Grosso State Brazilian Amazon Using Multisensor Datasets. *Remote Sens.* **2020**, *12*, 3827. [CrossRef]
10. Humber, M.L.; Boschetti, L.; Giglio, L.; Justice, C.O. Spatial and temporal intercomparison of four global burned area products. *Int. J. Digit. Earth* **2018**, *12*, 460–484. [CrossRef] [PubMed]
11. Lizundia-Loiola, J.; Pettinari, M.L.; Chuvieco, E. Temporal Anomalies in Burned Area Trends: Satellite Estimations of the Amazonian 2019 Fire Crisis. *Remote Sens.* **2020**, *12*, 151. [CrossRef]
12. Franquesa, M.; Stehman, S.V.; Chuvieco, E. Assessment and characterization of sources of error impacting the accuracy of global burned area products. *Remote Sens. Environ.* **2022**, *280*, 113214. [CrossRef]
13. Balch, J.K.; Abatzoglou, J.T.; Joseph, M.B.; Koontz, M.J.; Mahood, A.L.; McGlinchy, J.; Cattau, M.E.; Williams, A.P. Warming weakens the night-time barrier to global fire. *Nature* **2022**, *602*, 442–448. [CrossRef] [PubMed]
14. Fan, S.; Zhang, G.; Dennison, G.H.; FitzGerald, N.; Burn, P.L.; Gentle, I.R.; Shaw, P.E. Challenges in Fluorescence Detection of Chemical Warfare Agent Vapors Using Solid-State Films. *Adv. Mater.* **2020**, *32*, e1905785. [CrossRef] [PubMed]
15. Bountzouklis, C.; Fox, D.M.; Di Bernardino, E. Environmental factors affecting wildfire-burned areas in southeastern France, 1970--2019. *Nat. Hazards Earth Syst. Sci.* **2022**, *22*, 1181–1200. [CrossRef]
16. ANA Bacias Hidrográficas Ottocodificadas (Níveis Otto 1–7). Available online: https://metadados.snirh.gov.br/geonetwork/srv/api/records/b228d007-6d68-46e5-b30d-a1e191b2b21f (accessed on 15 January 2024).
17. IPAN Instituto de Pesquisa Ambiental Da Amazônia. 81% Do Desmatamento No Cerrado Se Concentrou Em Cinco Bacias Hidrográficas. Available online: https://ipam.org.br/81-do-desmatamento-no-cerrado-em-2023-foi-concentrado-em-cinco-bacias-hidrograficas/?gad_source=1&gclid=EAIaIQobChMItZOi5-2zhgMVZAutBh0NfQMxEAAYASAAEgKj3fD_BwE (accessed on 31 May 2024).
18. INPE. Brazilian Multi-Mission Platform -MMP AMAZONIA-1 Descritivo da Missão e do Satélite AMAZONIA 1: Descritivo da Missão e do Satélite. 2024. Available online: http://www.inpe.br/amazonia1/arquivos/A800000-DDD-001_v01-AMAZONIA_1-Descritivo_da_Missao_e_do_Satelite.pdf (accessed on 19 March 2024).
19. United States Geological Survey. Heart Explorer Data System. Base de dados 2019. USA. 2019. Available online: https://earthexplorer.usgs.gov/ (accessed on 19 March 2024).
20. INPE. Instituto Nacional de Pesquisas Espaciais, Dados Abertos, Programa Queimadas. 2024. Available online: https://terrabrasilis.dpi.inpe.br/queimadas/portal/dados-abertos/#da-area-qmd (accessed on 19 March 2024).
21. Libonati, R.; DaCamara, C.C.; Setzer, A.W.; Morelli, F.; Melchiori, A.E. An Algorithm for Burned Area Detection in the Brazilian Cerrado Using 4 µm MODIS Imagery. *Remote Sens.* **2015**, *7*, 15782–15803. [CrossRef]
22. Mapbiomas. MapBiomas Brasil. 2024. Available online: https://brasil.mapbiomas.org/metodo-mapbiomas-fogo/ (accessed on 19 March 2024).
23. Mann, H.B. Nonparametric tests against trend. *Econom. J. Econom. Soc.* **1945**, *13*, 245–259. [CrossRef]
24. Kendall, M.G.; Stuart, A.; Ord, J.K.; Arnold, S. *Kendall's Advanced Theory of Statistics: Classical Inference and the Linear Model*; Arnold: London, UK, 1999; Volume 2A.
25. Li, B.; Zhou, W.; Zhao, Y.; Ju, Q.; Yu, Z.; Liang, Z.; Acharya, K. Using the SPEI to Assess Recent Climate Change in the Yarlung Zangbo River Basin, South Tibet. *Water* **2015**, *7*, 5474–5486. [CrossRef]
26. Şen, Z. Innovative Trend Analysis Methodology. *J. Hydrol. Eng.* **2012**, *17*, 1042–1046. [CrossRef]
27. Berhail, S.; Tourki, M.; Merrouche, I.; Bendekiche, H. Geo-Statistical Assessment of Meteorological Drought in the Context of Climate Change: Case of the Macta Basin (Northwest of Algeria). *Model. Earth Syst. Environ.* **2021**, *8*, 81–101. [CrossRef]
28. Ronneberger, O.; Fischer, P.; Brox, T. U-Net: Convolutional Networks for Biomedical Image Segmentation. In *Medical Image Computing and Computer-Assisted Intervention—MICCAI 2015*; Navab, N., Hornegger, J., Wells, W., Frangi, A., Eds.; Springer: Cham, Switzerland, 2015; Volume 9351. [CrossRef]
29. Adrian, J.; Sagan, V.; Maimaitijiang, M. Sentinel SAR-optical fusion for crop type mapping using deep learning and Google Earth Engine. *ISPRS J. Photogramm. Remote Sens.* **2021**, *175*, 215–235. [CrossRef]
30. Wang, X.; Hu, Z.; Shi, S.; Hou, M.; Xu, L.; Zhang, X. A deep learning method for optimizing semantic segmentation accuracy of remote sensing images based on improved UNet. *Sci. Rep.* **2023**, *13*, 7600. [CrossRef]
31. Wen, Y. Based on the improved depth residual Unet high-resolution remote sensing road extraction method. In Proceedings of the Fourth International Conference on Geology, Mapping, and Remote Sensing (ICGMRS 2023), Wuhan, China, 14–16 April 2023; 129780E (2024). Volume 12978. [CrossRef]
32. Park, S.; Song, A. Shoreline Change Analysis with Deep Learning Semantic Segmentation Using Remote Sensing and GIS Data. *KSCE J. Civ. Eng.* **2023**, *28*, 928–938. [CrossRef]
33. Maxwell, A.E.; Warner, T.A. Thematic Classification Accuracy Assessment with Inherently Uncertain Boundaries: An Argument for Center-Weighted Accuracy Assessment Metrics. *Remote Sens.* **2020**, *12*, 1905. [CrossRef]

34. Biederman, J.A.; Robles, M.D.; Scott, R.L.; Knowles, J.F. Streamflow Response to Wildfire Differs with Season and Elevation in Adjacent Headwaters of the Lower Colorado River Basin. *Water Resour. Res.* **2022**, *58*, e2021WR030687. [CrossRef]
35. Brasil Decreto No 63.778, de 11 de Dezembro de 1968. Available online: https://www2.camara.leg.br/legin/fed/decret/1960-1969/decreto-63778-11-dezembro-1968-405144-publicacaooriginal-1-pe.html#:~:text=Disp%C3%B5e%20sobre%20a%20inclus%C3%A3o%20de%20munic%C3%ADpios%20na%20%C3%A1rea%20do%20Pol%C3%ADgono%20das%20Secas (accessed on 31 May 2024).
36. Alves, J.E.; Gonçalves, S.; Augusto, S. Precipitação Na Bacia Hidrográfica Do Rio Cachoeira, Nordeste Do Brasil: Tendências E Variabilidade (1970-2020). *Boletim do Museu Paraense Emílio Goeldi* **2022**, *17*, 527–542. [CrossRef]
37. Moreira de Araújo, F.; Ferreira, L.G.; Arantes, A.E. Distribution Patterns of Burned Areas in the Brazilian Biomes: An Analysis Based on Satellite Data for the 2002–2010 Period. *Remote Sens.* **2012**, *4*, 1929. [CrossRef]
38. Colli, G.R.; Vieira, C.R.; Dianese, J.C. Biodiversity and Conservation of the Cerrado: Recent Advances and Old Challenges. *Biodivers. Conserv.* **2020**, *29*, 1465–1475. [CrossRef]
39. World Metereological Organization. WMO statement on the status of the global climate in 2010. *World Meteorol.* **2011**, *1074*, 20.
40. Da Silva, E.M.; Carvalho, H.C.M.; da Silva, L.L.; Barbosa, W.A. Registros de Queimadas Em Vegetação (Incêndios) E a Climatologia Da Chuvas No Estado Do Ceará: Estudo de Caso No Período de 2015 a 2019. *Rev. Bras. De Meteorol.* **2021**, *36*, 571–577. [CrossRef]
41. Klink, C.A.; Sato, M.N.; Cordeiro, G.G.; Ramos, M.I.M. The Role of Vegetation on the Dynamics of Water and Fire in the Cerrado Ecosystems: Implications for Management and Conservation. *Plants* **2020**, *9*, 1803. [CrossRef]
42. Grisa, C. O Agronegócio E Agricultura Familiar No Planejamento Setorial Nos Governos FHC, Lula E Dilma: Continuidades E Descontinuidades. *Estud. Soc. E Agric.* **2021**, *29*, 545–573. [CrossRef]
43. Da Silva, P.; Sauer, S. Desmantelamento E Desregulação de Políticas Ambientais E Apropriação Da Terra E de Bens Naturais No Cerrado. *Raízes* **2022**, *42*, 298–315. [CrossRef]
44. da Silva, A.L.; Eloy, L.; Oliveira, K.R.; Coelho Filho, O.; Beltrão, M.R. Environmental Policy Reform and Water Grabbing in an Agricultural Frontier in the Brazilian Cerrado. *IDS Bull.* **2023**, *54*, 89–106. [CrossRef]
45. De Medeiros, M.B.; Miranda, H.S. Mortalidade Pós-Fogo Em Espécies Lenhosas de Campo Sujo Submetido a Três Queimadas Prescritas Anuais. *Acta Bot. Bras.* **2005**, *19*, 493–500. [CrossRef]
46. Aragão, L.E.O.C.; Shimabukuro, Y.E.; Cardoso, M.; Anderson, L.O.; Lima, A.; Poulter, B. Frequência de queimadas durante as secas recentes. In *Secas na Amazônia: Causas e Consequências*; Borma, L.D.S., Nobre, C.A., Eds.; Oficina de Textos: São Paulo, Brazil, 2013.
47. Silva, P.S.; Rodrigues, J.A.; Santos, F.L.M.; Pereira, A.A.; Nogueira, J.; DaCamara, C.C.; Libonati, R. Drivers of Burned Area Patterns in Cerrado: The Case of Matopiba Region. Available online: https://ieeexplore.ieee.org/document/9165665 (accessed on 15 January 2024).
48. Segura-Garcia, C.; Bauman, D.; Arruda, V.L.S.; Alencar, A.; Menor, I.O. Human Land Occupation Regulates the Effect of the Climate on the Burned Area of the Cerrado Biome. Available online: https://meetingorganizer.copernicus.org/EGU24/EGU24-10377.html (accessed on 5 June 2024).
49. Gonçalves, D.N.; Marcato, J.; Carrilho, A.C.; Acosta, P.R.; Paula, A.; David, F.; Osco, L.P.; da Rosa Oliveira, M.; Martins, J.A.C.; Damasceno, A.D.; et al. Transformers for Mapping Burned Areas in Brazilian Pantanal and Amazon with PlanetScope Imagery. *Int. J. Appl. Earth Obs. Geoinf.* **2023**, *116*, 103151. [CrossRef]
50. Wu, B.; Zheng, H.; Xu, Z.; Wu, Z.; Zhao, Y. Forest Burned Area Detection Using a Novel Spectral Index Based on Multi-Objective Optimization. *Forests* **2022**, *13*, 1787. [CrossRef]
51. Kouadio, B.K.; Ouattara, S.; Clément, A.; Zaouri, J.-M.G.B.; Jean-Luc, J.-L.K.K.; N'guessan, E.K. Detection of Burned Areas through Spectral Indices Analysis of Sentinel-2A Satellite Images in the Abokouamékro Wildlife Reserve (Central, Côte D'Ivoire). *Open J. Appl. Sci.* **2023**, *14*, 205–222. [CrossRef]
52. de Oliveira, L.M.; Galvão, L.S.; Ponzoni, F.J. Effects on the Determination of Hyperspectral Vegetation Indices: A Case Study in Southeastern Brazil. *Geocarto Int.* **2019**, *36*, 2186–2203. [CrossRef]
53. Santana, N.C.; de Carvalho Júnior, O.A.; Gomes, R.A.T.; Guimarães, R.F. Accuracy and Spatiotemporal Distribution of Fire in the Brazilian Biomes from the MODIS Burned-Area Products. *Int. J. Wildland Fire* **2020**, *29*, 907. [CrossRef]
54. Melchiorre, A.; Boschetti, L. Global Analysis of Burned Area Persistence Time with MODIS Data. *Remote Sens.* **2018**, *10*, 750. [CrossRef]
55. de Carvalho, I.S.; Alvarado, S.T.; Sanna Freire Silva, T.; Leandro de Oliveira Cordeiro, C.; Fidelis, A.; Valéria Carvalho Saraiva, R.; Figueiredo, F.A.M.M.A.; Roberto P. de Sousa, J.; Massi Ferraz, T. How Does the Fire Regime Change after Creating a Protected Area in the Brazilian Cerrado? *J. Nat. Conserv.* **2023**, *71*, 126318. [CrossRef]
56. Alencar, A.A.C.; Arruda, V.L.S.; da Silva, W.V.; Conciani, D.E.; Costa, D.P.; Crusco, N.; Duverger, S.G.; Ferreira, N.C.; Franca-Rocha, W.; Hasenack, H.; et al. Long-Term Landsat-Based Monthly Burned Area Dataset for the Brazilian Biomes Using Deep Learning. *Remote Sens.* **2022**, *14*, 2510. [CrossRef]
57. Campagnolo, M.L.; Libonati, R.; Rodrigues, J.A.; Pereira, J.M.C. A comprehensive characterization of MODIS daily burned area mapping accuracy across fire sizes in tropical savannas. *Remote Sens. Environ.* **2021**, *252*, 112115. [CrossRef]
58. Piao, S.; Liu, J. Accuracy Improvement of UNet Based on Dilated Convolution. *J. Phys. Conf. Ser.* **2020**, *1345*, 052066. [CrossRef]

59. Arruda, V.L.S.; Piontekowski, V.J.; Alencar, A.; Pereira, R.S.; Matricardi, E.A.T. An alternative approach for mapping burn scars using Landsat imagery, Google Earth Engine, and Deep Learning in the Brazilian Savanna. *Remote Sens. Appl. Soc. Environ.* **2021**, *22*, 100472. [CrossRef]
60. Abedi, R. Application of multi-criteria decision making models to forest fire management. *Int. J. Geoheritage Parks* **2022**, *10*, 84–96. [CrossRef]
61. Abdollahi, A.; Yebra, M. Forest fuel type classification: Review of remote sensing techniques, constraints and future trends. *J. Environ. Manag.* **2023**, *342*, 118315. [CrossRef]